

Microphase Separation and Rheological Properties of Polyurethane Melts. 1. Effect of Block Length

Sachin Velankar and Stuart L. Cooper^{*,†}

Department of Chemical Engineering, University of Delaware, Newark, Delaware 19716

Received July 21, 1998; Revised Manuscript Received October 22, 1998

ABSTRACT: A series of polyesterurethanes with differing block length and constant composition have been synthesized for rheological studies. Hard segments based on isophorone diisocyanate and 1,4-butanediol and soft segments based on polycaprolactone to ensure high thermal stability and to prevent high melting point crystallinity enabled long-duration rheological characterization at high temperatures. DSC and SAXS revealed that, at any fixed temperature above the polyester melting point, the degree of microphase separation increased with block length, with the shortest block lengths being almost single-phase. Temperature-resolved SAXS experiments demonstrated gradual microphase mixing of the microphase-separated materials as the temperature increased. In addition, the SAXS data for one material were shown to obey the predictions of the mean field theory, allowing a mean field estimate of the spinodal temperature to be calculated. Frequency sweep dynamic mechanical experiments show viscoelastic behavior characteristic of a homopolymer for all materials at high temperatures, and master curves can be constructed using the principle of time–temperature superposition. A failure of time–temperature superposition was observed at lower temperatures in materials with large block length. Temperature-resolved SAXS studies suggest that this failure is related to the onset of microphase separation in these materials at low temperatures. In the high-temperature regime, where master curves can be constructed, the WLF equation with universal parameters fits the experimental shift factors very well if an apparent single-phase glass transition temperature (T_g) is used. In addition, the relaxation time and the Newtonian viscosity of the polyurethanes show a strong dependence on block length, with a power law exponent of about 5.

Introduction

Polyurethanes^{1,2} (PUs) are an important class of thermoplastic elastomer with wide applications as coatings, binder resins, fibers, and high-performance elastomeric products. Typical PU elastomers are multiblock copolymers comprised of alternating “soft” polyether or polyester segments and “hard” polyurethane segments. The thermodynamic incompatibility of these segments, often combined with crystallization of either or both segments, drives their microphase separation into hard and soft phases that are respectively below and above their glass transition temperatures. This microphase separation is responsible for the excellent elastomeric properties of polyurethanes.

The solid-state properties of polyurethanes have been studied extensively over the past three decades. In contrast, melt studies of PUs have been relatively rare. The primary reason for this is that most commercial PUs are based on 4,4'-methylene bis(diphenyl diisocyanate) (MDI) and 1,4-butanediol (BD) hard segments, with a crystalline melting point of over 200 °C, or other hard segments with high glass transition temperatures. The aromatic urethane linkage is not stable at temperatures above about 130 °C,^{3–5} and thus long-duration melt experiments with commercial PUs are not feasible. Thus short-duration experiments such as DSC,^{6–10} synchrotron scattering,^{11–14} and infrared spectroscopic^{15–19} studies have been performed, but there are almost no data available on the viscoelastic behavior and relaxation phenomena in PU melts.

Perhaps the most detailed high-temperature study of a polyurethane was conducted by Koberstein^{8,11} et al.

using a commercial PU based on polytetramethylene oxide (PTMO) soft segments and MDI/BD hard segments. The major conclusions of those studies were that PUs show multiple endotherms between the soft-segment glass transition and the hard-segment melting temperature. The first endotherm occurs about 20 °C above the annealing temperature of the polymer and was ascribed to local rearrangements in the hard phase. The endotherms at the highest temperatures were ascribed to crystalline melting of the hard segments. Combined DSC and SAXS studies showed that an endotherm at intermediate temperatures was associated with microphase mixing, i.e., the sample underwent a microphase separation transition (MST) upon raising the temperature, and the authors were successful in constructing phase diagrams of some of the materials. Similar data have been reported earlier by Wilkes and Emerson²⁰ and later by Li et al.¹³

Such MSTs have been observed very commonly in diblock and triblock copolymers by scattering,^{21–23} calorimetry,^{24,25} and rheological^{26–28} studies. A key feature of such MSTs is the dramatic change in rheological properties at the transition. Specifically, the modulus of the polymer is known to change discontinuously at the MST, along with an abrupt failure of the principle of time–temperature superposition.^{26,28,29} Clearly, the morphology of the polymer affects the relaxation behavior very strongly. While the existence of a MST in polyurethanes has been clearly demonstrated beyond doubt,^{11,14,20} the resulting effect on viscoelastic properties has not been studied in detail.

Most viscoelastic property measurements of PUs at high temperatures have employed temperature-sweep dynamic mechanical analysis (DMA).^{30,31} Such experiments have usually been carried out in tensile mode and

[†] Present address: Department of Chemical Engineering, Illinois Institute of Technology, Chicago, IL 60616.

thus necessarily end when the sample begins to flow. They typically show a low soft-segment glass transition temperature, a rubbery plateau, and finally the hard-segment glass transition or crystalline melting above which sample flow occurs. Most of the remaining studies about relaxation in PUs employed nuclear magnetic resonance (NMR),^{32,33} dielectric spectroscopy,^{34,35} which is of interest in insulation and solid-state sensor applications, or mechanical spectroscopy,^{36,37} which is of interest for elastomeric or vibration damping applications. At the low temperatures employed in these studies, the hard phase can, for all practical purposes, be considered to be immobile, and these may be regarded as studies of relaxations of the physically cross-linked soft-segment phase. As such, these studies have little relevance to the present work.

There has been at least one attempt to correlate viscoelastic properties of PUs to their microphase separation transition. Ryan¹⁴ and co-workers studied a PU based on PTMO and mixed 2,4'- and 4,4'-MDI/BD hard segments and compared the results of SAXS experiments with those of dynamic mechanical experiments. The major conclusions of the SAXS experiments were similar to those of Koberstein, revealing that the systems studied underwent microphase mixing at about 150 °C, as measured by a decrease in the SAXS invariant. Dynamic mechanical testing in shear was successfully performed (as already noted, DMA in the tensile mode is not useful for melt studies), and the authors demonstrated a 10-fold decrease in the storage modulus in the temperature range corresponding to microphase mixing. The focus of their study was the microphase mixing of the PU and not rheological characterization; in any case, due to the high hard-segment T_g of these materials, detailed rheological characterization was not possible.

Before proceeding, an important observation made by Ryan et al.¹⁴ deserves mention. Ryan et al. observed that a higher order peak has never been reported in any publication regarding small-angle scattering studies of polyurethanes. This is in stark contrast to diblock and triblock copolymers, where several higher order reflections can be easily seen in scattering data.²³ The inevitable conclusion of this observation is that the lamellar phase of polyurethanes does not possess long-range crystal-like order. Spatial correlation within the lamellar morphology extends only over a few lamellae, and lamellar stacks of tens of lamellae characteristic of the lamellar phase in most diblock and triblock copolymers have not been seen. This idea is clearly represented in the drawings of polyurethane morphology constructed by Koberstein.¹¹ Thus, following Adams²³ et al., this paper makes a distinction between an order-disorder transition (ODT) and an MST. For the majority of diblock and triblock copolymers studied so far, microphase separation also corresponds to onset of long-range order. On the other hand for polyurethanes, an MST has been seen^{11,14,20} without observation of an ODT.

This paper describes recent observations about the rheological properties of PU elastomers that have been specifically designed for rheological studies. There are three key variables that control the structure and properties of PU elastomers: block length, block incompatibility, and composition. Each of these in turn was varied to examine their effects on the resultant mechanical relaxation spectrum of the PUs. The results of

Table 1. Materials

designation	soft segment MW	soft segment wt fraction	weight-average MW
E830	830	0.47	31 000
E1250	1250	0.51	32 000
E2000	2000	0.52	71 000
E3000	3000	0.53	77 000
IPDI/BD		0	116 000

the first of these three variables, block length, are presented here, keeping the block incompatibility and the composition constant. On the basis of the studies of degradation of the urethane linkage,³⁻⁵ purely aliphatic urethanes are most likely to remain stable at high temperatures. In addition, since it is desirable to achieve a melt at low temperatures, the glass transition temperature must be low and there should be no high-melting point crystallinity in the hard segments. Hard segments based on isophorone diisocyanate (IPDI) and 1,4-butanediol (BD) satisfy all these criteria and have been selected for the present family of materials. To cover a range of morphologies from microphase mixed to microphase separated, polycaprolactone diol (PCL) has been selected as the soft segment; the high polarity of PCL ensures that it will be miscible with the hard segments, at least at low block lengths. PCL is known to crystallize; however, these crystals melt below 50 °C; therefore, all polymers have been held at 55 °C prior to experiments to avoid effects of crystallinity. At present, we wish to avoid complicating data analysis with entanglement issues; fortunately, no evidence of entanglement was found in these materials, despite the fact that all have molecular weights over 30 000.

Experimental Section

Polycaprolactone diols (Scientific Polymer) of various molecular weights and 1,4-butanediol (Aldrich Chemical Co.) were dried in a vacuum for several hours before use. Isophorone diisocyanate and dibutyltin dilaurate (Aldrich) were used as received. Solution polymerizations were conducted following standard methods³⁸ using *N,N*-dimethylacetamide (DMAc) as solvent and dibutyltin dilaurate as catalyst. The temperature was kept low (<55 °C) during these polymerizations to prevent any cross-linking side reactions. The polymers were precipitated in distilled water and dried in a vacuum at 0.1 Torr, 50 °C for at least 2 days. The polymers were redissolved in DMAc to approximately 15 wt %, filtered, and cast onto Teflon plates. The solutions were dried at 45–50 °C for 3–4 days and then in a vacuum for a further 3–4 days to obtain films of about 0.5 mm thickness which were stored in desiccators.

Molecular weights were measured by gel permeation chromatography (GPC) using mixed-bead columns (Polymer Laboratories) and a Hewlett-Packard refractive index detector. Samples were dissolved to about 0.1 wt % in DMAc, and monodisperse polystyrene standards were used for calibration. Several samples were recovered after rheological or scattering experiments at high temperature for extended periods and their GPC traces compared with those before experiments. The traces were found to be identical, indicating no molecular weight degradation under the experimental conditions used. Identical GPC traces were also observed for samples held in air at 140 °C for 2 h. Any dissociation of the urethane in the presence of moisture will cause molecular weight degradation; clearly, there is no significant relaxation of stress due to bond scission in the rheological experiments. The molecular weights and various other characteristics of the materials used in this study are presented in Table 1; all materials in this study had approximately 50 wt % of soft segments and polydispersity indices between 1.5 and 1.8.

The compositions of the materials were determined using quantitative ¹³C NMR on a 240 MHz instrument (Bruker). The

PUs were dissolved in deuterated dimethyl sulfoxide, and the NMR experiments were carried out at 60 °C with a data acquisition delay of 30 s.

DSC experiments were performed on a Perkin-Elmer DSC 7 cooled with liquid nitrogen using hermetically sealed sample pans and samples weighing 10–15 mg. The DSC was calibrated using indium and mercury. The DSC sample holder was enclosed in a drybox purged with nitrogen to prevent moisture condensation. DSC scans of dried, as-cast samples showed polycaprolactone crystalline melting that was completed below 50 °C in all samples. Recrystallization did not occur, even after storage at room temperature for 1 week. All samples were exposed to the same thermal history of annealing at 55 °C for 22–24 h prior to any other experiments.

SAXS experiments were performed using Cu K α radiation from a rotating anode generator (Rigaku), a compact Kratky camera for collimation, and a 1-D proportional gas-filled wire detector (Braun OED-50M). Detector sensitivity and linearity were measured by irradiating 0.001 in. stainless steel shim-stock and employing the excited fluorescence as an isotropic source. The sample to detector distance (~350 mm) was measured using the first three peaks of cholesteryl myristate. Absolute intensity calibration was performed using a Lupolen 1029 standard calibrated at the Oak Ridge National Laboratory (ORNL). Samples were taped with Kapton tape to minimize sample flow and held in a home-built temperature cell to within 0.1 °C of the set temperature. Each sample was measured at least three times and transmittance was measured before and after each data acquisition to verify that sample flow had not occurred. The Kratky camera was purged with helium throughout the scattering experiment to minimize air scattering. The collected data were subjected to empty beam subtraction, smoothed, and finally desmeared using an iterative algorithm by Lake.³⁹ The background was assumed to have the form

$$I_b(q) = a + bq^4 \quad (1)$$

The second term in **1** is the form suggested by Vonk⁴⁰ for the leading edge of any wide-angle scattering. In addition, the scattered intensity was assumed to have high- q behavior following Porod's form:⁴¹

$$I(q) = I_{\text{obs}}(q) - I_b(q) = cq^{-4} \quad (2)$$

Porod's form is strictly valid for ideal two-phase systems with sharp interfaces, and it is unlikely that the present materials satisfy this criterion. Various researchers^{42–44} have suggested other forms for the scattering in the high- q region that attempt to include the effect of finite interface width. Nevertheless, Porod's form has been used here since it fits the data perfectly, leaving no additional information to reliably obtain additional parameters related to the interface width. Thus, the observed intensities at high q were fit to $a + bq^4 + cq^{-4}$ using gnuplot, a nonlinear least squares regression software package, and $I_b(q)$ was subtracted to obtain the scattered data. Calculation of correlation functions and invariants involves extrapolation of measured data to both high as well as low q . The high q data were assumed to follow Porod's law, as described above. The low q data often follow Guinier's law⁴⁵

$$I(q) = I(q=0) \exp\left(-\frac{q^2}{R_g^2}\right) \quad (3)$$

where R_g is the radius of the gyration of the scatterer. In the present work, most samples show severely curved Guinier plots of $\ln I(q)$ vs q^2 , indicating that eq 3 does not describe the low- q scattering. A commonly used form for scattering data that show an upturn in the scattered intensity at low- q , as shown by the present samples, is a Lorentzian function⁴¹

$$I(q) = \frac{I(0)}{(q^2 + k^2)} \quad (4)$$

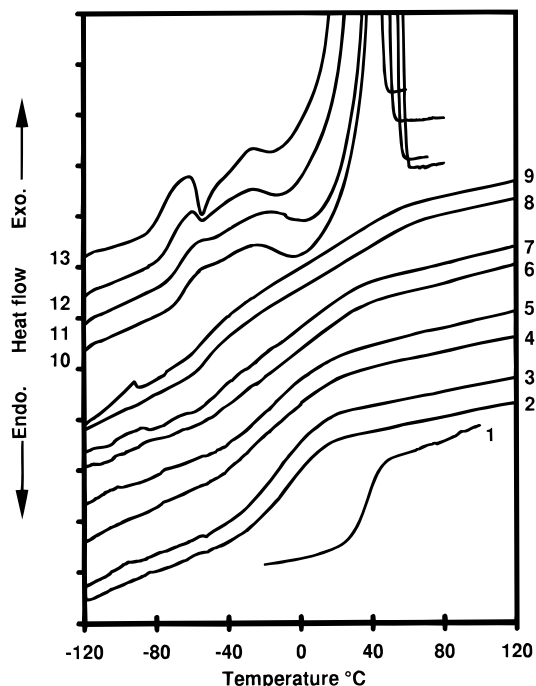


Figure 1. DSC results for polyurethanes and homopolymer: curve 1, IPDI/BD hard segment; curves 2 and 3, E830; curves 4 and 5, E1250; curves 6 and 7, E2000; curves 8 and 9, E3000; curves 10, 11, 12, and 13, PCL with MWs 830, 1250, 2000, and 3000, respectively, quenched from 100 °C; curves 2, 4, 6, and 8, samples annealed at 55 °C overnight; curves 3, 5, 7, and 9, samples annealed at 55 °C overnight and 200 °C for 4 min before test. Each division on the y axis is 0.1 W/g.

where $1/k$ is the correlation length in the system. Plots of $1/I(q)$ vs q^2 yielded straight lines; however, the intercept, $k^2/I(0)$, was often found to be negative, which is unphysical.

Hence, extrapolation of the data to low q has been avoided altogether, and all integrals have been truncated above 0.07 nm⁻¹. This causes negligible error in the calculated invariants; however, it affects the correlation function at large distances quite significantly.

Dynamic mechanical temperature sweep experiments were performed on a Rheometrics RSA-II tensile-strain-controlled instrument at a frequency of 80 rad/s between -150 °C and sample flow temperatures. The instrument boils off liquid nitrogen to use as coolant, and thus, the samples remained under nitrogen at all times.

Dynamic mechanical frequency sweep experiments were performed on a Rheometrics RMS-800 strain-controlled rheometer under nitrogen flow using 25 mm parallel plate geometry. All experiments were performed in the linear-viscoelastic region, and changes in the gap due to thermal expansion were accounted for. Samples were allowed to equilibrate at each temperature for at least 10 min before collecting data between 0.01 and 100 rad/s. Data were collected in 10 °C increments, and each data set was the average of at least three specimens. To obtain data in reduced form, the principle of time-temperature superposition⁴⁶ was applied after a vertical shift of T/T_{ref} , where $T_{\text{ref}} = 90$ °C was chosen arbitrarily. Each frequency-modulus curve was superposed upon the corresponding data at the next higher temperature; whenever curves could not be superposed over the entire frequency range, superposition at high frequency was carried out.

Results and Discussion

DSC Data. Qualitative Assessment. Figure 1 shows the DSC data for all samples as well as for the homopolymer soft segments; these data have been summarized in Table 2. The PCL homopolymers were

Table 2. Thermal Characteristics of Polyurethanes

sample	pure homopolymer properties						polyurethane properties						calculated properties			
	pure homopolymer properties			polyurethane properties			polyurethane properties				calculated properties					
	$T_{g,ss}$, °C	$\Delta C_{p,ss}$, J/g	corrctd $\Delta C_{p,ss}$, J/g ^a	$T_{g,hs}$, °C	$\Delta C_{p,hs}$, J/g	$T_{g,mid}$, °C	$T_{g,onset}$, °C	ΔC_p , J/g	W_{ss}^b	ΔC_p , ^c J/g	T_g , ^d °C	f_{ss}^e	F_{ss}^f	T_g for WLF fit, °C		
E830	-75.5 ± 1	0.21 ± 0.03	0.47	36.0 ± 2	0.43 ± 0.05	-9 ± 5	-33 ± 2.5	0.43 ± 0.02	0.47	0.45	-18.7	0.38	0.97	-18.4		
E1250	-71.5 ± 1	0.17 ± 0.03	0.38	36.0 ± 2	0.43 ± 0.05	-10 ± 7	-45 ± 3	0.40 ± 0.07	0.51	0.40	-15.3	0.46	0.99	-11.4		
E2000	-67.0 ± 1	0.15 ± 0.01	0.33	36.0 ± 2	0.43 ± 0.05	<i>g</i>	-52 ± 2.5	0.11 ± 0.06 ^f	0.52	0.38	-11.0			-10.4		
E3000	-63.5 ± 1	0.15 ± 0.01	0.33	36.0 ± 2	0.43 ± 0.05	-52 ± 1.5	-63 ± 1.5	0.13 ± 0.01	0.47	0.38	-4.5	0.91	0.38	0.6		

^a Corrected for crystallinity, as explained in the text. ^b Measured by quantitative ¹³C NMR; expected error ~3%. ^c From Couchman's equation (5), assuming no microphase separation. ^d From Couchman's equation (6). ^e From eq 7. ^f From eq 8. ^g Transition is too poorly defined to measure reliably.

quenched from their melt state at 100 °C before recording the data. Upon reheating, a low-temperature transition is observed, followed by a small crystallization exotherm and then a melting endotherm that is far more intense than the crystallization exotherm. This indicates that the sample undergoes considerable crystallization during the quench from the melt at 100 °C.

No such crystallization is seen in any of the PU samples, in fact, as previously mentioned, the samples remain noncrystalline, even if stored at room temperature for several days. Sample E830 shows no feature other than a single broad glass transition. E1250 also shows a single transition that is probably too broad to be a single relaxation process. Samples E2000 and E3000 show transitions at much lower temperatures which are characteristic of a microphase-separated polyurethane. The midpoints of the glass transitions of E830 and E1250 are not highly reproducible, due to their very large breadth; hence, Table 2 also lists the onsets of these transitions, which are more reproducible. As expected, the onset temperatures decrease with increasing block length, approaching the T_g of the pure soft segment. This has commonly been regarded indicative of increasing phase purity.

Figure 1 also shows that annealing at 200 °C for 4 min causes almost no change in the DSC curves; i.e., the phase compositions are the same at 200 °C as at 55 °C. This is a somewhat surprising result and more comments on this will be made at the end of this paper. It should be noted that these quench results, particularly for E3000, were not highly reproducible. Some quenches of E2000 and E3000 showed T_g s several degrees higher than those shown in Figure 1.

DSC Data. Quantitative Analysis. The Couchman⁴⁷ equations have often been used to describe the glass transitions of blends and block copolymers in the single-phase state. These equations state that the ΔC_p at the T_g is a weighted sum of the ΔC_p s of the pure components

$$\Delta C_p = w_{ss}\Delta C_{p,ss} + w_{hs}\Delta C_{p,hs} \quad (5)$$

and provide an expression for the T_g of a single-phase blend

$$T_g = \frac{w_{ss}T_{g,ss} + \alpha w_{hs}T_{g,hs}}{w_{ss} + \alpha w_{hs}} \quad (6)$$

where w_{ss} and w_{hs} are the soft- and hard-segment weight fractions in the sample and $\alpha = \Delta C_{p,hs}/\Delta C_{p,ss}$ is the ratio of the specific heat changes for the pure components.

Equation 6 can be applied to estimate the composition of a specific phase of a microphase-separated sample from its measured T_g , after inverting it to get

$$f_{ss} = \frac{\alpha(T_{g,hs} - T_g)}{(T_{g,ss} - T_g) + \alpha(T_{g,hs} - T_g)} \quad (7)$$

where f_{ss} is the weight fraction of the soft segment in the soft-segment phase.

Finally, soft segments that are dissolved in the hard phase are assumed to have no contribution at all to the soft-segment glass transition, and thus, the weight fraction of the soft-segment phase is given by

$$F_{ss} = \frac{\Delta C_p}{f_{ss}\Delta C_{p,ss} + (1 - f_{ss})\Delta C_{p,hs}} \quad (8)$$

The $\Delta C_{p,ss}$ in the above equations refers to pure amorphous PCL, since no crystalline melting is seen on reheating the quenched samples. On the other hand, the pure PCL homopolymers show considerable crystallization during the quench, as mentioned above. Thus, the $\Delta C_{p,ss}$ measured (and listed in the third column of Table 2) refers to the amorphous portion of the quenched sample and is an underestimate. To correct these values, the degree of crystallinity in the quenched samples must first be estimated from the net specific heat of melting (i.e. the difference between the areas under the melting and the crystallization peaks). This net specific heat of melting was found to be 74 ± 2 J/g for all four molecular weights. Then, using the specific heat of melting of crystalline PCL (135 J/g),⁴⁸ a degree of crystallinity of 55% was calculated for the quenched PCL homopolymers and used to find the corrected $\Delta C_{p,ss}$ values in column 4 of Table 2.

The calculated values of Table 2 show that the measured ΔC_p s of E830 and E1250 are very close to those calculated assuming a single-phase sample. In contrast, the measured values for E2000 and E3000 are appreciably lower than those calculated, implying that only a part of the total soft segment contributes to the soft-segment glass transition; the rest is mixed with the hard-segment phase and plays no role in the soft-segment transition. Table 2 also shows that the T_g s calculated assuming single-phase samples are also comparable to the measured values for E830 and E1250 but much higher for E2000 and E3000. More comments will be made on these calculated T_g s in the rheology section.

Equations 7 and 8 are used to find the fraction of soft segment in the soft-segment phase and the weight fraction of the soft-segment phase listed in Table 2. These results, at least for E830 and E1250, are altogether unphysical; for the soft-segment phase, $f_{ss} > w_{ss}$ must hold, by definition; moreover, F_{ss} values close to 1 are unreasonable. The most likely source of this error is the assumption that the soft segments dissolved in the hard-segment phase do not contribute to the soft-

segment T_g . This assumption has been found to be valid in polyurethanes, where the hard-segment T_g is high (above 100 °C). In the present case with $T_{g,hs} = 36$ °C, there may be sufficient soft-segment mobility in the hard-segment phase to allow it to contribute to ΔC_p at the soft-segment glass transition.

To summarize, we conclude that, as observed by DSC, E830 and E1250 are in a single-phase state, whereas E2000 and E3000 are progressively more microphase-separated.

Small-Angle X-ray Scattering. SAXS Theory for Polyurethanes. SAXS is useful for elucidating the structure of multiphase materials in the size range of about 2–200 nm. Most quantitative analysis is based upon models of the morphology which may be very detailed ones that predict the scattering profile or some general assumptions that predict specific features of the scattering curves, such as limiting behavior at low or high q and integrated scattering intensity. Most typical polyurethanes show small-angle scattering profiles with a single Bragg peak,^{31,44} and the most common assumption is one of a lamellar morphology, allowing at least the long spacing (interlamellar distance) to be calculated. Depending on the quality of data and the availability of other information, other morphological details such as width of interfaces and microphase compositions may be calculated.

The long spacing, d , may be calculated using the Bragg law⁴¹

$$d = 2\pi/q_{\max} \quad (9)$$

where q_{\max} is the position of the maximum in the Lorentz-corrected scattering intensity, i.e., $q^2 I(q)$ vs q . It may also be calculated from the first maximum in the one-dimensional correlation function⁴⁰

$$\gamma(x) = \frac{1}{Q} \int_0^\infty I(q) q^2 \cos(qx) dq \quad (10)$$

where the SAXS invariant, Q is related to $\overline{\Delta\rho^2}$, the mean square electron density fluctuations in the system as

$$Q = \int_0^\infty I(q) q^2 dq = 2\pi^2 \overline{\Delta\rho^2} \quad (11)$$

A qualitative analysis of the correlation function indicates the degree of order in the system. A sharp Bragg peak gives a correlation function with several maxima, indicating long-range order, whereas a diffuse Bragg peak gives a correlation function that dies off after a single peak, indicating that order is lost after only a few lamellae.

If the material were completely phase-separated, the electron densities of the two phases, ρ_{ss} and ρ_{hs} , could be used to calculate the invariant of an ideal two-phase system

$$Q_{\max} = 2\pi^2 \phi_{ss} \phi_{hs} (\rho_{ss} - \rho_{hs})^2 \quad (12)$$

where ϕ_{ss} and ϕ_{hs} are the volume fractions of the soft and hard phases, respectively.

The ratio Q/Q_{\max} has often been used as a measure of the degree of phase separation in polyurethanes.^{31,38,49} Quantitatively useful calculation of the degree of phase separation requires accurate measurements of the

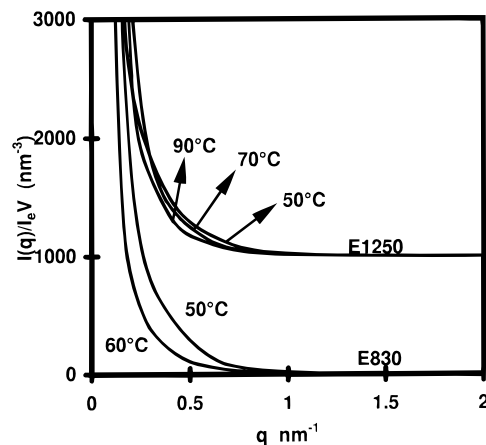


Figure 2. SAXS data for E830 and E1250. E1250 curves have been moved by 1000 nm⁻³ in the y direction for clarity.

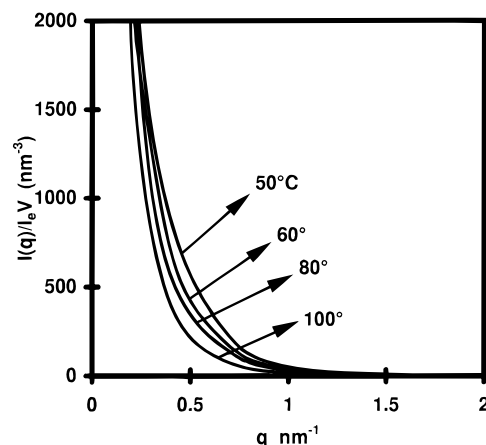


Figure 3. SAXS data for E2000.

absolute intensity of the samples as well as of the densities and the volume fractions of each phase.

SAXS Data Analysis. Figure 2 shows the SAXS patterns for E830 and E1250. Both of these samples show very little scattering, the intensity of which seems to reduce slightly with temperature. These samples scatter weakly, and the scattering is comparable to that of the Kapton tape used to prevent sample flow. Moreover, data acquisition times are very limited due to sample flow, since these samples are viscous above 50 °C. Thus, these data are difficult to reproduce, and no analysis of these curves was attempted. These data are presented here to corroborate the conclusion of the DSC data that both E830 and E1250 are almost single-phase materials.

Figure 3 shows the SAXS data for E2000 at various temperatures. In this case, scattering is much stronger and can be easily reproduced, at least up to 80 °C. The trend of decreasing scattering is unmistakable, especially in the Lorentz-corrected data of Figure 4. At 50 °C, the broad Bragg peak has a maximum at about $q = 0.47$ nm⁻¹, which corresponds to a long spacing of 13.5 nm; at high temperatures the peak is not sufficiently well-defined to allow determination of the long spacing with great confidence.

Figure 5 shows the SAXS patterns of E3000, where a Bragg peak is clearly visible at 50 °C and decreases monotonically with temperature until it is barely visible as a shoulder at 120 °C. However, the same data after Lorentz correction (Figure 6) show that the Bragg peak does not altogether vanish, even at the highest temper-

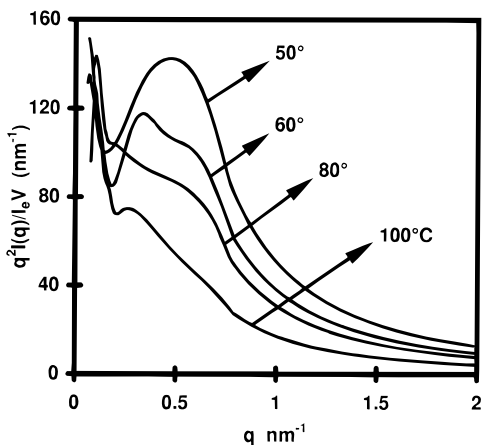


Figure 4. SAXS data for E2000 after Lorentz correction.

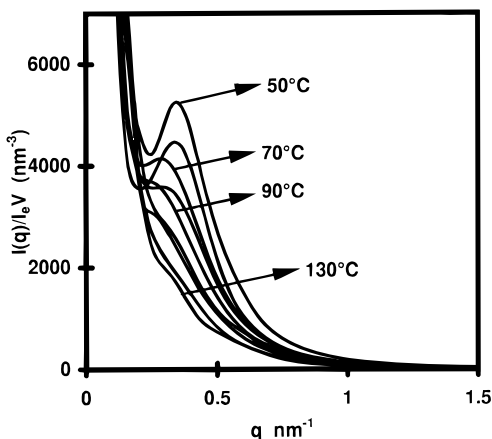


Figure 5. SAXS data for E3000. The topmost curve is at 50 °C, and the temperature rises by 10 °C for each successive curve below.

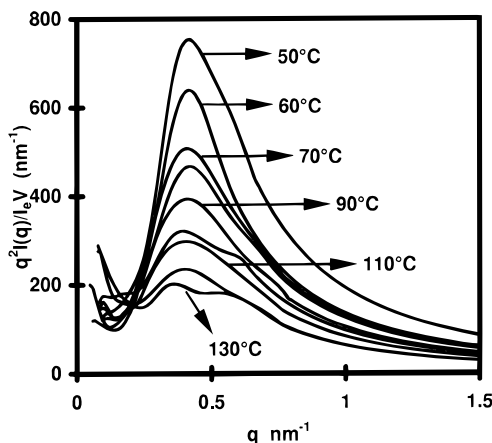


Figure 6. SAXS data for E3000 after Lorentz correction. The topmost curve is at 50 °C, and the temperature rises by 10 °C for each successive curve below.

atures. Above 110 °C, scattering is too weak and sample flow too fast to allow high reproducibility of data; nevertheless, the presence of significant scattering is not in doubt. The presence of a scattering peak is, of course, not conclusive evidence of microphase separation, and other factors, such as excluded volume effects (correlation hole scattering),⁵⁰ can also give rise to a scattering peak, even if the sample is single-phase. Another source of scattering is concentration fluctuations in the melt.⁵¹ As mentioned earlier, polyurethanes

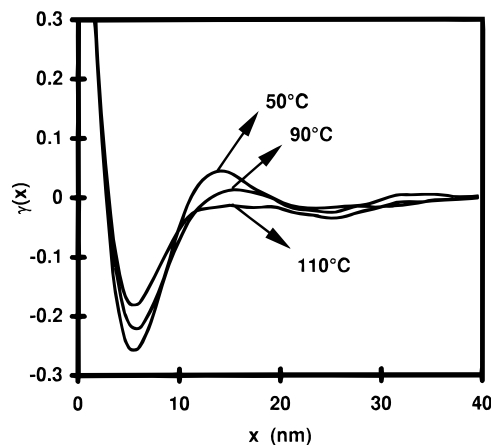


Figure 7. One-dimensional correlation function for E3000 at selected temperatures.

are fairly disordered materials, and the long-range crystalline ordering characteristic of diblock and triblock copolymers has never been seen in PUs. Thus, we see no reason to distinguish concentration fluctuations from microphase separation and take the naïve viewpoint that concentration fluctuations are merely a weak version of microphase separation.

The maximum in the scattering profile is between 0.4 and 0.42 nm⁻¹ at all temperatures, although the peak is found to be appreciably broader at high temperatures. This corresponds to a long spacing of 15.3 nm for E3000 independent of temperature. A more quantitative analysis of the scattering profiles based on various theories^{52,53} was not attempted due to the poor statistical quality of the data.

Figure 7 compares the correlation function of E3000 at selected temperatures. First, even at 50 °C, the correlation function shows only a faint second maximum between 30 and 35 nm, indicating poor long-range lamellar order. Second, the heights of both maxima reduce as temperature increases, indicating a more disordered structure at higher temperatures. We reiterate that the correlation functions of Figure 7 are not very accurate at large distances since the truncation of the intensity below $q = 0.07 \text{ nm}^{-1}$ causes errors that increase significantly with x .

To estimate ρ_{ss} and ρ_{hs} , we use

$$\rho_{\text{phase}} = \frac{(\text{electrons/repeat unit})(\text{density of phase})N_{\text{Av}}}{\text{Molecular wt of repeat unit}} \quad (13)$$

The density of the IPDI/BD homopolymer was measured by immersion in aqueous sodium chloride solutions at 25 °C and was found to be $1.109 \pm 0.005 \text{ g/cm}^3$. Due to rapid absorption of water by polycaprolactone, this immersion technique is not suitable for pure polycaprolactone, or for the polyurethanes. Hence, a density of 1.09 g/cm^3 for amorphous PCL at room temperature, listed in the *Polymer Handbook*⁴⁸ was used. Thus from eq 13, we estimate ρ_{ss} to be 357 electrons/nm³ and ρ_{hs} to be 364 electrons/nm³, i.e., a very poor electron density contrast. This calculation is somewhat pessimistic, since at room temperature, E3000 shows an invariant 50% higher than that calculated from the above electron densities; nevertheless, the electron density contrast is far weaker than in most polyurethanes. In addition, measurement of densities of these materials at high temperatures is difficult and

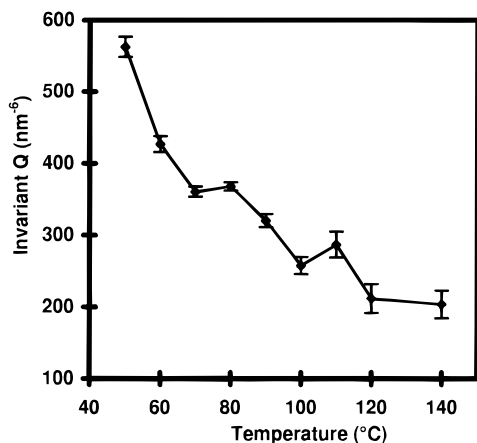


Figure 8. SAXS invariant for E3000.

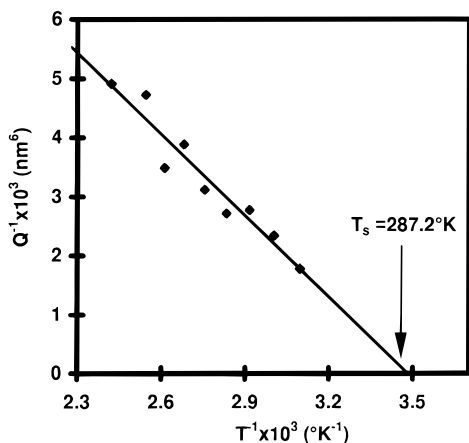


Figure 9. Mean field theory estimate for spinodal temperature of E3000.

was not attempted. In light of these facts, quantitative calculations of the degree of phase separation in these systems were not attempted. Instead, Figure 8 plots the invariant of E3000 as a function of temperature without normalization with an ideal invariant Q_{\max} . The decrease in the invariant by a factor of more than 2 between 50 and 140 °C is a quantitative measure of microphase mixing.

The data of Figure 8 are displayed in Figure 9 in the form of Q^{-1} vs T^{-1} . (The conventional form is one of reciprocal of maximum in intensity vs T^{-1} ; however, in the present case, the peaks are not well-defined at high temperatures. Since all peaks can be superimposed upon each other by scaling the intensity, the invariant is an equivalent and more reliable measure of the peak intensity.) These data are fitted to a straight line as demanded by mean field theory and extrapolated to $Q^{-1} = 0$ to get the mean field estimate of the spinodal temperature, $T_s = 14$ °C. By this yardstick, E3000 should be regarded as being above the MST at all the temperatures studied. Figure 10 then tests another prediction of the mean field theory:

$$I(q_{\max}) = \left(1 - \frac{T_s}{T}\right)^{-\gamma} \quad \text{where } \gamma = 1 \quad (14)$$

Considering the possible errors in calculating the absolute intensities and the numerous assumptions made in applying mean field theory to this system, the agreement between the experimental $\gamma = 0.969 \pm 0.05$ with the mean field prediction is excellent.

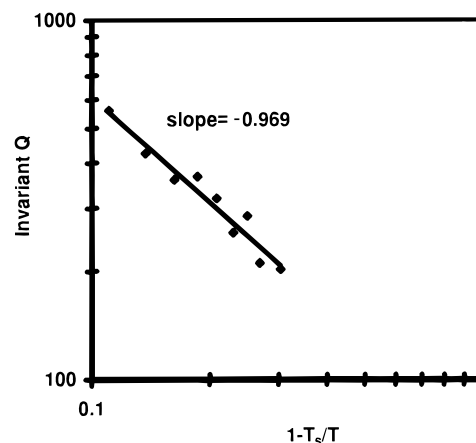


Figure 10. A test of mean field theory for E3000; the theoretically predicted slope is 1.

As an aside, apart from the change in microphase compositions, the difference in the thermal expansion coefficients of the two phases also affects the electron density difference, and hence the SAXS invariant. In the present case, this is expected to be a minor effect, since a difference in thermal expansion coefficients would also cause a change in the Bragg spacing, which has not been observed. (Moreover, there is very little difference in the invariant at room temperature and at 50 °C, which further suggests that thermal expansion effects are not dominant). Thus, the change in invariant in Figure 8 is, to a large part, due to changes in the extent of phase separation.

Finally, all the scattering data of Figures 2, 3, and 5 show that scattering intensity increases at very low q and that this scattering increases with temperature. This upturn in scattering at small angles is observed (and highly reproducible), even at low temperatures at which sample flow does not occur, allowing accurate measurement of sample transmittance. Even at higher temperatures, this upturn is far too strong to be explained away by errors in measurement of transmittance. We believe that this feature is not artifactual and that the upturn in scattering increases with temperature. It is possible that this upturn is due to scattering of individual "grains" of microphase-separated material; on the other hand, small dust particles or air bubbles are also known to produce an upturn at low angles. A similar feature was observed by Ryan et al.¹⁴ and ascribed to bubble formation.

Rheological Properties. Temperature Sweep Dynamic Mechanical Tests. Figure 11 shows results of the most traditional means of measuring viscoelastic properties of PUs, viz., temperature sweep dynamic mechanical experiments at high frequency (here 80 rad/s) in tensile mode. Only two samples are shown; E830 was found to be too soft to be held in the jaws of the instrument and E2000 had properties intermediate to those of E1250 and E3000 and has been omitted for clarity. The data for both samples show a peak in E'' at about -130 °C that has been attributed to local, crankshaft-type motions of the methylene sequences in soft segment. At higher temperatures, E1250 shows a single glass transition at about -16 °C (maximum in E') followed by sample flow at room temperature. E3000 shows a much lower T_g of about -41 °C, followed by a slight plateau in E' , followed by sample flow at about 50 °C. These features manifest themselves as a shoulder in the $\tan \delta$ plot at about -40 °C, which is usually

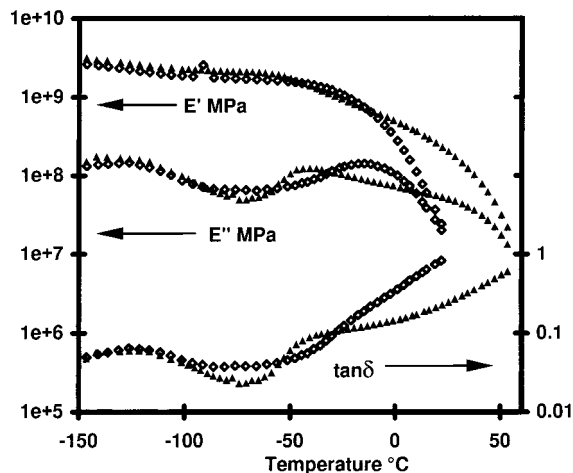


Figure 11. Dynamic mechanical temperature sweep data in tensile mode. E2000 shows behavior intermediate to that of E1250 and E3000; E830 is too soft to be tested.

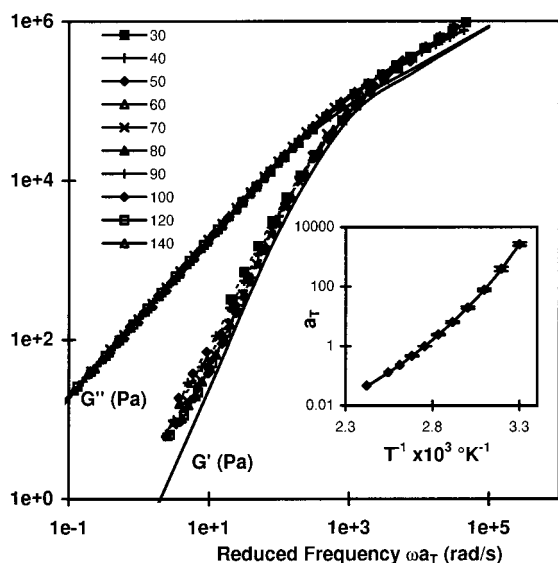


Figure 12. Dynamic mechanical frequency sweep data for E830. The solid line is a fit to the Rouse theory. The inset shows the shift factors used for time-temperature superposition; the error bars are smaller than the symbols used. The solid line in the inset is the WLF equation.

regarded as the most easily identifiable signature of microphase separation in PUs. As mentioned in the Introduction, tensile tests necessarily stop when the polymer flows and thus are impractical for melt rheological studies. Moreover, tensile tests are not suitable for measurement at low frequencies, since the stress relaxes over the time scale of a single measurement.

Frequency Sweep Dynamic Mechanical Tests. Much more fundamental information can be obtained by frequency sweep dynamic mechanical tests at various temperatures, and each sample is considered in turn below.

E830. Figure 12 shows the modulus-reduced frequency curve for E830. The solid line is an approximate fit to the Rouse model;⁴⁶ details for obtaining this fit are mentioned later in the paper. There are substantial quantitative deviations from the Rouse predictions; nevertheless, the data qualitatively show all the features of the Rouse model, including the correct terminal slopes of 1 and 2 for G'' and G' , as well as a slope of 0.5 at high frequency. The inset shows the shift factors used

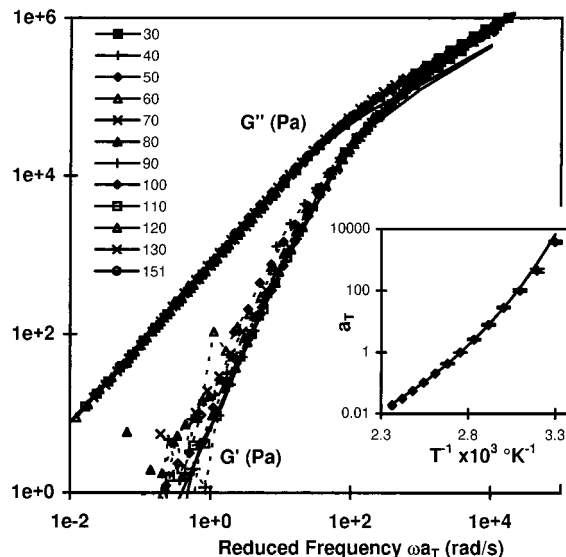


Figure 13. Dynamic mechanical frequency sweep data for E1250. The solid line is a fit to the Rouse theory. The inset shows the shift factors used for time-temperature superposition. The solid line in the inset is the WLF equation.

to construct Figure 2. The Williams-Landel-Ferry (WLF) equation⁴⁶

$$\log(a_T) = \frac{-C_{1g}(T - T_g)}{C_{2g} + T - T_g} \quad (15)$$

has been used successfully for several homopolymers, where the subscript g refers the shift factor to the glass transition temperature and the values $C_{1g} = 17.66$ K and $C_{2g} = 51.6$ K work well for many polymers. Since the reference temperature of 90 °C was chosen arbitrarily, a_T was calculated using

$$\log(a_T) = \log(a_{T_g}) - \log(a_{T_{ref}}) \quad (16)$$

where a_T refers to the shift factors of Figure 2 and $a_{T_{ref}}$ is the shift factor at $T_{ref} = 90$ °C.

For a PU, the glass transition temperature in this context is ill-defined, since the soft phase and the hard phase have T_g s that are often separated by more than 100 °C. For E830 this problem is not severe, since it shows a single broad T_g as mentioned earlier; however, this is not true for all the samples presented in this paper. Hence, T_g has been used as a fitting parameter to get the solid line in the inset of Figure 2 at a T_g value of -18.4 °C. This is somewhat lower than the thermal T_g of -9 °C noted in Table 2 but equal to that calculated from the pure component T_g s assuming a single-phase sample.

E1250. The viscoelastic properties of E1250 are shown in Figure 13. All the comments made for Figure 2 are valid for E1250 as well, except that superposition of G' does not work as well as it does for E830. The solid line in the inset of Figure 4 is a fit to eqs 1 and 2 with a T_g of -11.4 °C, which is almost equal to the thermal T_g noted in Table 2 and well within the error in the calculated value.

E2000. As seen in Figure 14, E2000 behaves similarly to the previous two samples at and above 80 °C. However, at lower temperatures, time-temperature superposition breaks down, more so for G' than for G'' . On the relatively large scale of Figure 14, this break-

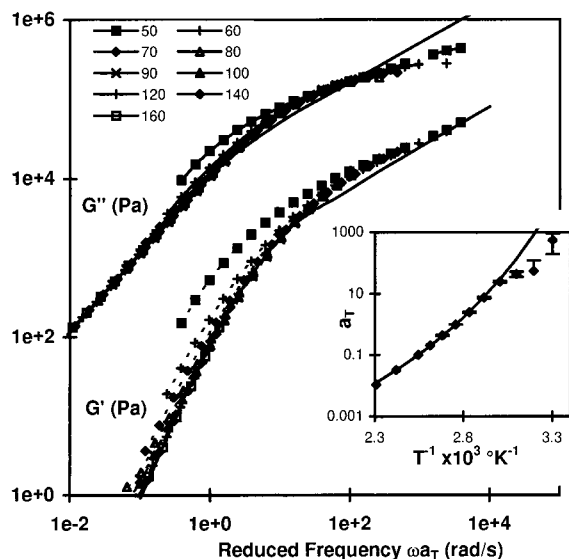


Figure 14. Dynamic mechanical frequency sweep data for E2000. G' data have been reduced by a factor of 20 for clarity. The solid line is a fit to the Rouse theory. The inset shows the shift factors used for time-temperature superposition. The solid line in the inset is the WLF equation.

down is clearly visible only at 50 °C: however, superposition is not valid at 60 and 70 °C as well. This breakdown of superposition is much more obvious for E3000 and is discussed in the next section.

The solid line in the inset of Figure 14 is a fit to eqs 1 and 2 with $T_g = -10.4$ °C. The thermal T_g of this sample is not sufficiently well-defined to be measured, yet judging by the trend in the onsets of the transitions of all four samples, we may expect that the T_g of E2000 is well below -10 °C. A similar discrepancy occurs between the thermal glass transition and the best fit parameter for E3000 as well; a possible reason for this discrepancy is proposed later in this paper. On the other hand, Couchman's prediction⁴⁷ for the single-phase T_g is in excellent agreement with the fitted value of -10.4 °C.

E3000. The breakdown of time-temperature superposition is much more evident for this sample, as seen in Figure 15. Such a breakdown has been observed in several diblock and triblock copolymer systems,^{26,28,29} where modulus-reduced frequency data show two separate branches above and below a certain temperature range. In Figure 15, the modulus-reduced frequency curves at the two lowest temperatures superimpose completely, suggesting that there may be a low-temperature branch of the kind observed in diblock and triblock copolymers. Attempts to investigate this further failed, since data collected at lower temperatures for E3000 (as well as E2000) were not highly reproducible. The solid line in the inset of Figure 15 was calculated using a T_g of 0.6 °C, which is somewhat higher than the single-phase T_g of -4.5 °C calculated from Couchman's equation but well within the experimental error of measuring T_{gs} , ΔC_p s, and compositions. Thus fairly good agreement is found between last column of Table 2 with Couchman's predicted T_{gs} for all four samples. Clearly, in the high-temperature range where time-temperature superposition works, the rheological behavior is similar to that of single-phase materials, both in the qualitative shape of the master curves as well as in the quantitative use of the WLF equation with a predicted single-phase T_g .

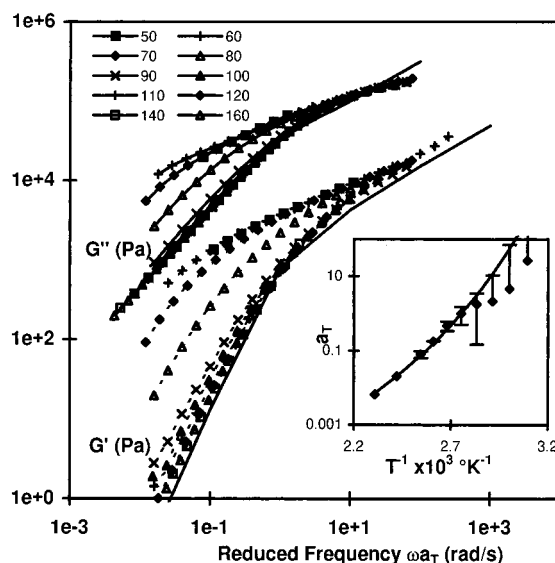


Figure 15. Dynamic mechanical frequency sweep data for E3000. G' data have been reduced by a factor of 20 for clarity. The solid line is a fit to the Rouse theory. The inset shows the shift factors used for time-temperature superposition. The solid line in the inset is the WLF equation.

In several diblock and triblock copolymers, this breakdown of superposition has been shown to be related to a microphase separation transition.^{26,28,29} Evidence of gradual microphase mixing has already been demonstrated in the SAXS section, and we therefore conclude that microphase separation at low temperatures is responsible for the breakdown of superposition in the present polyurethanes as well. Two facts deserve additional comment: First, phase mixing in E3000 is spread over an extremely wide range in temperatures. This is somewhat at variance from the observations for diblock and triblock copolymers in which order-disorder transitions or order-order transitions tend to be very sharp, with their width limited only by instrument resolution.²⁹ This could be happening for several reasons, the most important of which is polydispersity; polyurethanes are far more polydisperse than diblock copolymers made by anionic polymerization. This is true for overall polydispersity as well as for block polydispersity. Thus, the broad MST observed here corresponds to the phase compositions gradually approaching each other till the contrast is too poor to be seen in scattering experiments.

Second, judging from the SAXS data, even at the highest temperature studied, E3000 is not completely microphase mixed. Despite this, it obeys time-temperature superposition above 100 °C, with terminal behavior characteristic of a liquid sample ($\log G' \propto \omega^2$). This is not true in microphase-separated diblock and triblock copolymers, where terminal behavior usually follows $\log G' \propto \omega^b$ with $b = 0.5$ ²⁶ (though values from 0.2 to 0.7 have been reported).²⁸ The most probable explanation of this is that microphase separation alone is not sufficient to prevent the terminal behavior characteristic of a liquid. As mentioned in the Introduction, in most diblock and triblock copolymers, an MST is also an ODT, i.e., long-range order is essential to observe terminal behavior different from a liquid. This was most clearly demonstrated by Adams et al.²⁸ in a kinetic study of highly asymmetric styrene-isoprene diblock and triblock copolymers. They showed that a frequency sweep experiment conducted after microphase separation but

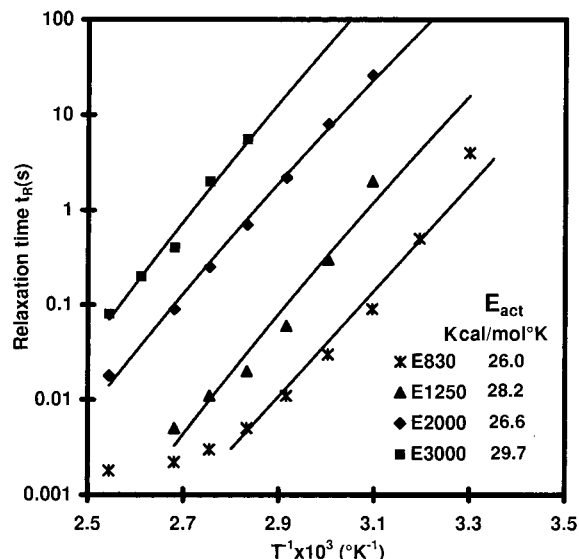


Figure 16. Relaxation times for the polyurethanes: dependence on temperature. Solid lines are fits to the Arrhenius equation with activation energies listed in the legend.

before ordering gave liquidlike terminal behavior with $G' \sim \omega^2$, but the same sample, after ordering on a body-centered cubic lattice, gave a much lower terminal slope. Thus, in the present case, the E3000 is a disordered liquid beyond a length scale of a few lamellae and behaves as such.

Relaxation Times and Molecular Weight Dependence. The Rouse model may be fitted to the raw modulus–frequency data (i.e. prior to shifting) at each temperature to obtain a relaxation time at each temperature. This fitting involves two parameters: the terminal viscosity, η_0 , and the longest relaxation time, t_R . The viscosity can be obtained directly and reliably from the G' data in the terminal region, leaving t_R as the only fitting parameter. At high temperatures, excellent fits are obtained and, as expected, the relaxation times agree with the a_T vs temperature plots. At low temperatures, fits to Rouse theory are not very good; nevertheless, the longest relaxation time has been extracted from the data at all temperatures where G' shows terminal behavior (allowing the viscosity η_0 to be reliably determined). These relaxation times are considerably longer than those predicted from a_T plots, since the time–temperature superposition fails at low frequencies, and it is the low-frequency data that are relevant to the longest relaxation time. (The solid lines in Figures 12–15 were constructed by using the relaxation time for the entire master curve; these are very close to those obtained at 90 $^{\circ}\text{C}$.) These relaxation times are plotted as a function of temperature in Figure 16 and as a function of block length in Figure 17. Figure 16 shows that the relaxation times increase with block length, even at the highest temperatures studied. This seems inconsistent with a completely homogeneous melt in which rheological properties may be expected to be independent of block length. Thus we propose that these polymers are very weakly segregated at high temperatures. Mechanical relaxation then involves soft blocks moving between soft-segment-rich domains by diffusing through hard-segment-rich domains, and thus, longer blocks may be expected to have longer relaxation times. This mechanism is consistent with the SAXS data that show weak scattering at all temperatures. One could alternately interpret it as an effect of increasing con-

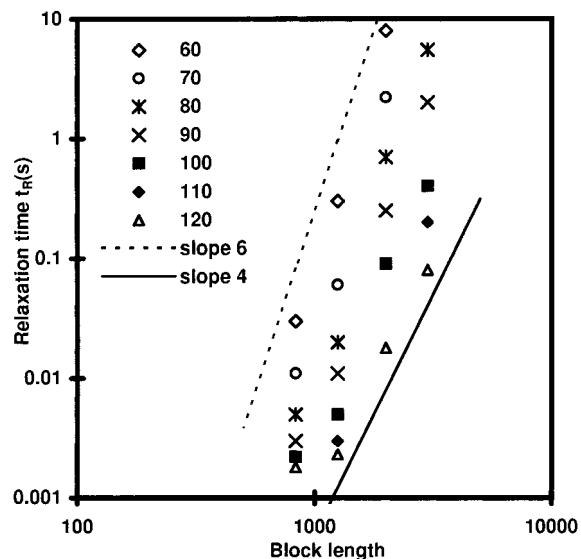


Figure 17. Relaxation times for the polyurethanes: dependence on block length.

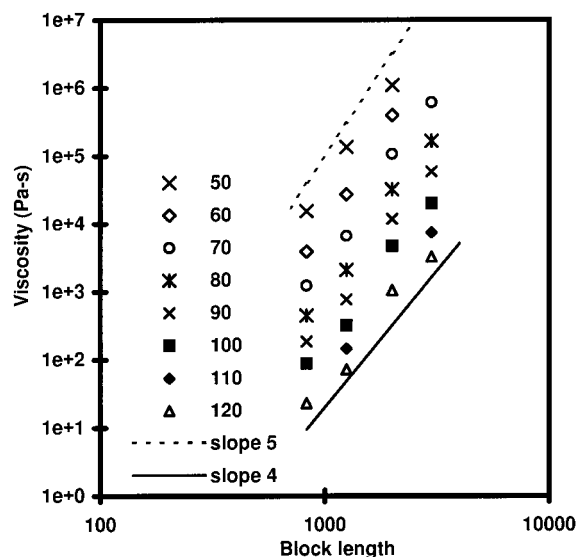


Figure 18. Terminal viscosity of polyurethanes: dependence on block length.

centration fluctuations in the melt as block length increases; as mentioned earlier, this paper makes no distinction between concentration fluctuations and microphase separation. However, the temperature dependence of the relaxation time is similar for all samples; in fact, if we insist on fitting the data of Figure 16 to the Arrhenius equation, all four samples show almost the same activation energy. This is somewhat surprising, since the activation energy for the mechanism of chain motion described above may also be expected to increase with block length. (Note that the possibility of relaxation by chemical bond scission has been ruled out in the GPC section). Perhaps the most important feature of Figure 17 is that the dependence of t_R on block length is extremely severe, with an exponent ranging from 4 to 6. While there is considerable arbitrariness in extracting a relaxation time from the low-temperature data, the strong dependence is not in doubt. A similar strong dependence on block length is noted for the Newtonian viscosity in Figure 18. The power law exponent reduces from about 4.9 to about 4 as temperature increases from 50 to 120 $^{\circ}\text{C}$.

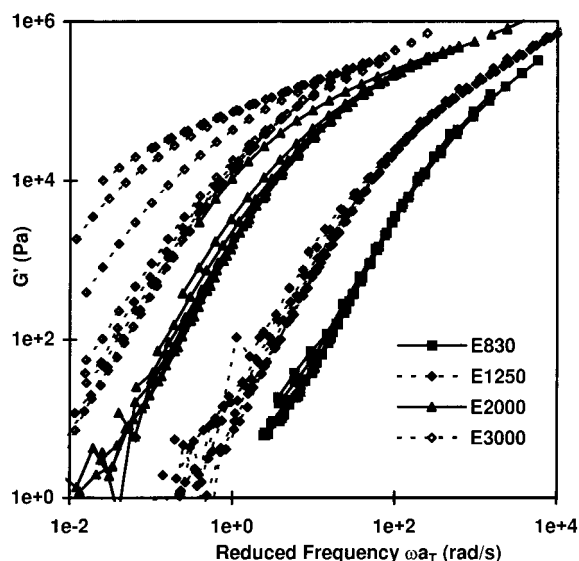


Figure 19. Effect of block length on the storage modulus of polyurethane melts.

Finally, Figure 19 plots all the G' vs reduced frequency data in Figures 12–15 in order to judge the effect of increasing block length. Clearly, the master curves in the high-temperature region where time-temperature superposition is valid are very similar in shape, suggesting a “time-block length superposition” at high temperatures. In fact, if the reduced frequency were scaled by the Rouse time to construct Figure 19, the four master curves of modulus vs ωt_R superimpose completely.

It should be noted that Figures 16–18 cannot be constructed out of experiments with diblock or triblock copolymers. In those systems, an increase in block length at constant composition necessarily results in an increase in overall molecular weight, with dramatic effects on the relaxation time and viscosity. It is not possible to separate the effect of increase in block length from that of increase in overall molecular weight. On the other hand, it is possible to synthesize multiblock copolymers with fixed overall molecular weight but different block lengths. As long as the former is much larger than the latter, the two effects can be separated. We are aware that the present series of materials does not have constant molecular weight (see Table 1); controlling the overall MW of a polyurethane is not an easy and was not attempted. Fortunately, E830 and E1250 have almost identical molecular weight, as do E2000 and E3000, allowing them to be directly compared. That all four points lie on approximately straight lines (on a logarithmic plot) for all temperatures supports the view that the effect of block length dominates over that of overall molecular weight.

Summary and Conclusions

We have successfully completed dynamic mechanical characterization of noncrystalline PUs in the melt state. DSC, as well as SAXS, shows that E830 and E1250 are single-phase materials. Rheologically these samples to behave like homopolymer melts and obey the Rouse theory reasonably well. The DSC results for E2000 and E3000 show that they are increasingly microphase-separated and seem to remain so, even after quenching from 200 °C. If these samples were single-phase at 200 °C, they would have shown T_g s that were considerably

higher, and closer to the values predicted from Couchman's equation. SAXS data show that E2000 is almost single-phase above 90 °C, whereas E3000 is increasingly phase-mixed at higher temperatures, although complete phase mixing is not observed at the highest temperature studied. Finally, rheologically, E2000 behaves like a single-phase sample above 70 °C and E3000, above 100 °C. The WLF equation fits the observed shift factors at high temperature exactly if the T_g s predicted by Couchman's equation for equivalent single-phase materials are used. This indicates that in the high-temperature regime where rheological master curves can be constructed, the polymers behave like single-phase samples.

Finally the following discrepancy is addressed: DSC shows no evidence of phase mixing at all, whereas SAXS and rheological data show considerable evidence of phase mixing. The most likely explanation of this is that microphase separation of these polymers is so rapid that even the fastest DSC quench is not enough to “freeze” the structure at the annealing temperature. We are aware that this is a somewhat surprising conclusion in light of the numerous DSC studies^{11,14,54} that have successfully quenched PUs in a single phase from the melt. However, most of these studies used PUs based on MDI/BD, in which a high hard-segment T_g may have helped “freeze” the sample very early during the quench. The present PUs have a hard-segment T_g of 36 °C, keeping them in a mobile state for a considerably longer time. As noted in the DSC section, the quench data for samples E2000 and E3000 are not highly reproducible, and microphase separation during the quench may be the reason for this irreproducibility.

Acknowledgment. The financial support of the Army Research Office (Grant DAAH04-96-1-0428) is gratefully acknowledged.

References and Notes

- (1) Hepburn, C. *Polyurethane Elastomers*, 2nd ed.; Elsevier Applied Science: London, 1991.
- (2) Wirpsza, Z. *Polyurethanes: Chemistry, Technology and Application*; Horwood: New York, 1993.
- (3) Fabris, H. J. *Adv. Ureth. Sci. Technol.* **1978**, *6*, 173.
- (4) Wong, S. W.; Frisch, K. C. *Adv. Ureth. Sci. Technol.* **1981**, *8*, 75.
- (5) Simon, J.; Barla, F.; Haller, A. K.; Farkas, F.; Kraxner, M. *Chromatographia* **1988**, *25*, 99.
- (6) Seymour, R. W.; Cooper, S. L. *Macromolecules* **1973**, *6*, 19.
- (7) Bogart, J. W. C.v.; Bluemke, D. A.; Cooper, S. L. *Polymer* **1981**, *22*, 1428.
- (8) Leung, L. M.; Koberstein, J. T. *Macromolecules* **1986**, *19*, 706.
- (9) Koberstein, J. T.; Galambos, A. F. *Macromolecules* **1992**, *25*, 5618.
- (10) Chen, T. K.; Shieh, T. S.; Chui, J. Y. *Macromolecules* **1998**, *31*, 1312.
- (11) Koberstein, J. T.; Russell, T. P. *Macromolecules* **1986**, *19*, 714.
- (12) Gibson, P. E.; Bogart, J. W. C.v.; Cooper, S. L. *J. Polym. Sci., Polym. Phys. Ed.* **1986**, *24*, 885.
- (13) Li, Y.; Gao, T.; Linliu, K.; Desper, C. R.; Chu, B. *Macromolecules* **1992**, *25*, 7365.
- (14) Ryan, A. J.; Macosko, C. W.; Bras, W. *Macromolecules* **1992**, *25*, 6277.
- (15) Srichratapimuk, V. W.; Cooper, S. L. *J. Macromol. Sci. Phys.* **1978**, *B15*, 267.
- (16) Coleman, M. M.; Lee, K. H.; Skrovaneck, D. J.; Painter, P. C. *Macromolecules* **1986**, *19*, 2149.
- (17) Koberstein, J. T.; Gancarz, I.; Clarke, T. C. *J. Polym. Sci.: Part B: Polym. Phys.* **1986**, *24*, 2487.
- (18) Goddard, R. J.; Cooper, S. L. *Macromolecules* **1995**, *28*, 1390.
- (19) Teo, L. S.; Chen, C. Y.; Kuo, J. F. *Macromolecules* **1997**, *30*, 1793.
- (20) Wilkes, G. L.; Emerson, J. A. *J. Appl. Phys.* **1976**, *47*, 4261.
- (21) Bates, F. S.; Hartney, M. A. *Macromolecules* **1985**, *18*, 4278.
- (22) Sakamoto, N.; Hashimoto, T. *Macromolecules* **1995**, *28*, 6825.

- (23) Adams, J. L.; Quiram, D. J.; Graessley, W. W.; Register, R. A.; Marchand, G. R. *Macromolecules* **1996**, *29*, 2929.
- (24) Bates, F. S.; Bair, H. E.; Hartney, M. A. *Macromolecules* **1984**, *17*, 1987.
- (25) Morese-Seguela, B.; St-Jaques, M.; Renaud, J. M.; Prud'homme, J. *Macromolecules* **1980**, *13*, 100.
- (26) Bates, F. S. *Macromolecules* **1984**, *17*, 2607.
- (27) Sakamoto, N.; Hashimoto, T.; Han, C. D.; Kim, D.; Vaidya, N. Y. *Macromolecules* **1997**, *30*, 1621.
- (28) Adams, J. L.; Graessley, W. W.; Register, R. A. *Macromolecules* **1994**, *27*, 6026.
- (29) Rosedale, J. H.; Bates, F. S. *Macromolecules* **1990**, *23*, 2329.
- (30) Kajiyama, T.; MacKnight, W. J. *Trans. Soc. Rheo.* **1969**, *13*, 527.
- (31) Bogart, J. W. C.v.; Gibson, P. E.; Cooper, S. L. *J. Polym. Sci., Polym. Phys. Ed.* **1983**, *21*, 65.
- (32) Kintanar, A.; Jelinzki, L. W.; Gancarz, I.; Koberstein, J. T. *Macromolecules* **1986**, *19*, 1876.
- (33) Ishida, M.; Yoshinaga, K.; Horii, F. *Macromolecules* **1996**, *29*, 9.
- (34) Vallance, M. A.; Yeung, A. S.; Cooper, S. L. *Colloid Polym. Sci.* **1983**, *261*, 541.
- (35) Petrovic, Z. S.; Javni, I.; Banhegy, G. *J. Polym. Sci., Polym. Phys. Ed.* **1998**, *36*, 237.
- (36) Duffy, J. V.; Lee, G. F.; Lee, J. D.; Hartmann, B. In *Sound and Vibration Damping with Polymers*; Corasco, R. D., Sperling, L. H., Eds.; ACS Symposium Series: Washington D. C.; 1990; p 281.
- (37) Hartmann, B.; Lee, G. F. *J. Noncryst. Solids* **1991**, *131-133*, 887.
- (38) Miller, J. A.; Cooper, S. L. *J. Polym. Sci. Polym. Phys.* **1985**, *23*, 1065.
- (39) Lake, J. A. *Acta Crystallographica* **1967**, *23*, 191.
- (40) Vonk, C. G. *J. Appl. Crystallogr.* **1973**, *6*, 81.
- (41) Balta-Calleja, F. J.; Vonk, C. G. *X-ray Scattering of Synthetic Polymers*; Elsevier Science: Amsterdam, 1989.
- (42) Ruland, W. *J. Appl. Crystallogr.* **1971**, *4*, 70.
- (43) Koberstein, J. T.; Morra, B.; Stein, R. S. *J. Appl. Crystallogr.* **1980**, *13*, 34.
- (44) Koberstein, J. T.; Stein, R. S. *J. Polym. Sci., Polym. Phys. Ed.* **1983**, *21*, 2181.
- (45) Guinier, A.; Fournet, G. *Small-Angle Scattering of X-rays*; John Wiley and Sons: New York, 1955.
- (46) Ferry, J. D. *Viscoelastic Properties of Polymers*; John Wiley and Sons: New York, 1980.
- (47) Couchman, P. R. *Macromolecules* **1978**, *11*, 117.
- (48) Brandrup, J.; Immergut, E. H. *Polymer Handbook*, 3rd ed.; John Wiley and Sons: New York, 1989.
- (49) Leung, L. M.; Koberstein, J. T. *J. Polym. Sci., Polym. Phys. Ed.* **1985**, *23*, 1883.
- (50) Gennes, P. G. D. *Scaling Concepts in Polymer Physics*; Cornell University Press: Ithaca, 1979.
- (51) Fredrickson, G. H.; Helfand, E. *J. Chem. Phys.* **1987**, *87*, 697.
- (52) Dobrynin, A. V.; Leibler, L. *Macromolecules* **1997**, *30*, 4756.
- (53) Benoit, H.; Hadziioannou, G. *Macromolecules* **1988**, *21*, 1449.
- (54) Hu, W.; Koberstein, J. T. *J. Polym. Sci., Polym. Phys. Ed.* **1994**, *32*, 437.

MA9811472